FDTD Modeling of Gold Nanoparticles in a Nematic Liquid Crystal: Quantitative and Qualitative Analysis of the Spectral Tunability

Montacer Dridi and Alexandre Vial*

Institut Charles Delaunay - Université de technologie de Troyes - Laboratoire de Nanotechnologie et d'Instrumentation Optique - 12, rue Marie Curie BP-2060 F-10010 TROYES Cedex

Received: November 18, 2009; Revised Manuscript Received: April 21, 2010

In this paper we numerically investigate an active plasmonic device that is based on an ordered array of gold nanocylinders with an elliptic basis embedded in a nematic liquid crystal (LC) layer. The localized surface plasmon resonance (LSPR) of the gold cylinders depends on the refractive index of the surrounding media, which depends on the orientation of the optical axis. Rotating the optical axis causes the LSPR to shift, and we will show that by modifying geometrical parameters we can increase the sensitivity of the LSPR to the orientation of the optical axis and thereby enhance the switching effects.

Introduction

Plasmonic resonances in metallic structures are resulting from collective oscillations of surface conduction electrons interacting with light. It is a well-known phenomenon extensively studied and used in photonics, promising new optical elements.[1,2] These electron-photon excitations allow one to manipulate electromagnetic waves in compact subwavelength metallic structures as well as to achieve strong electromagnetic field confinement and enhancement.[2] The absorption peak caused by the localized surface plasmon (LSPR) is dependent on the size and shape of the metallic structure.[3−5]

The dielectric environment surrounding the metallic nanostructure plays another important role to affect the absorption peak of SPR. Varying the effective dielectric medium surrounding the nanostructures would shift the SPR modes.[6] One of the techniques to manipulate this refractive index uses the electro-optic effect exhibited, for example, by liquid crystal molecules. Liquid crystals are well-known through their use in display technology. Their refractive index depends on the molecular alignment, which can be modulated using an electric field. Using liquid crystal in combination with metallic nanostructures leads to hybrid electro-optic devices, that are very promising for engineering applications.

Some works have shown the effect of integration of liquid crystals with thin film metal/dielectric.[7,8] The effects of integration of liquid crystals with gold gratings,[9] gold nanoparticles,[10,11] gold nanodots,[12] gold nanorods,[13,14] gold nanodisk,[15,16] and nanohole arrays[17] have also been demonstrated in experiments. In a recent paper,[18] numerical investigation of arrays of metallic nanoparticles covered by a liquid crystal have been reported. It was demonstrated that by rotating the director, it is possible to modify the resonance of the system according to a simple law. The particules were cylinders with a circular basis. But as already mentioned, the shape of the structures as an influence on the LSPR tunability.

For these reasons, in this paper we specifically focus on studying the effects of the orientation of the LC molecules in tuning plasmon resonances for elongated gold particles. We will show how the geometrical parameters affect the spectral tunability (i.e., maximum of shift resulting by orientation of the director) and we will give qualitative explanations of these effects.

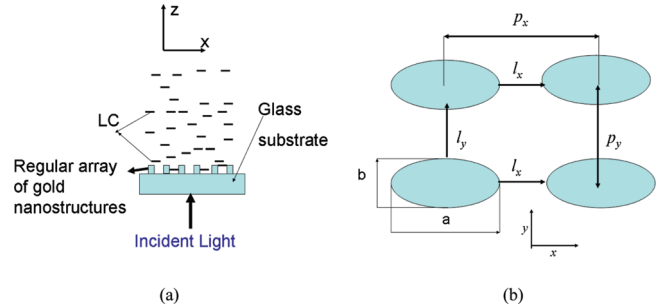

Figure 1. Schematic representation of gold nanocylinders with elliptic basis.

Description of the Structures of Interest

The nanoparticles we study are gold cylinders with an elliptic basis, the major axis has a length $a = 100$ nm (parallel to x-axis), the minor axis is $b = 50$ nm (parallel to y-axis), the height is $h = 50$ nm, and the periodicity of the array (distance center−center) is $p_x = p_y = 200$ nm. A schematic representation of gold nanocylinders with elliptic basis is presented in Figure 1.

These nanostructures are deposited on a glass substrate and embedded in a liquid crystal layer. As in our previous paper,[18] we consider a positive nematic crystal (uniaxial) with $n_o = 1.53$ (ordinary index) and $n_e = 1.74$ (extraordinary index). The LC in nematic phase have long-range orientational order that define their optical axis.[19]

Assuming the optical axis in the $x-z$ plane (Figure 2), we define θ as the angle between the optical axis and $\vec{z}$. The LC dielectric tensor expressed in the (x, y, z) basis is[20]

$$\varepsilon = \varepsilon_0 \begin{pmatrix} n_o^2 \cos^2\theta + n_e^2 \sin^2\theta & 0 & (n_o^2 - n_e^2)\sin\theta\cos\theta \\ 0 & n_o^2 & 0 \\ (n_o^2 - n_e^2)\sin\theta\cos\theta & 0 & n_o^2 \sin^2\theta + n_e^2 \cos^2\theta \end{pmatrix} \quad (1)$$

* To whom correspondence should be addressed: E-mail: alexandre.vial@utt.fr.

10.1021/jp910950m
Published on Web 05/06/2010

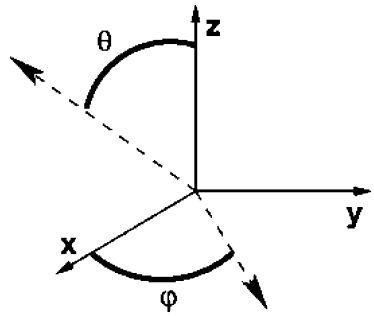

Figure 2. Geometry of the study. The angle between the optical axis and the z axis in the $x-z$ plane is denoted by θ. The angle between the optical axis and the x axis in the $x-y$ plane is denoted by ϕ.

If the optical axis is located in the (x, y) plane (Figure 2), we define ϕ as the angle between the optical axis and $\vec{x}$. The LC dielectric tensor expressed in the (x, y, z) basis is

$$\varepsilon = \varepsilon_0 \begin{pmatrix} n_e^2 \cos^2\phi + n_o^2 \sin^2\phi & (n_o^2 - n_e^2)\cos\phi \sin\phi & 0 \\ (n_o^2 - n_e^2)\cos\phi\sin\phi & n_e^2 \sin^2\phi + n_o^2 \cos^2\phi & 0 \\ 0 & 0 & n_o^2 \end{pmatrix} \quad (2)$$

The incident light is propagating along the z-direction and polarized along the x axis. The thickness of LC layer is 100 nm. The choice of this thickness will be justified later.

Description of the Numerical Method

Finite-difference time-domain (FDTD) is a computational method for solving Maxwell's equations. It is one of the most powerful and convenient method as solutions can cover a wide frequency range with a single simulation run. On the basis of second-order central differences, the FDTD method implements the space derivatives of the curl operators via finite differences in regular interleaved Cartesian space meshes for the electromagnatic fields. The original algorithm was introduced in ref 21 and was valid only for isotropic nondispersive materials.

But when metallic structures are studied in FDTD calculations, modifications of recursive equations are needed to account for the dispersive properties of such materials.[22] The FDTD algorithm that we use is based on the recursive convolution method.[23] This approach is used after fitting the complex dielectric function of metals with a set of Lorentzien and Drude poles. So we write the permittivity of gold as

$$\varepsilon_{DL} = \varepsilon_\infty - \frac{\omega_D^2}{\omega(\omega + j\gamma_D)} - \frac{\Delta\varepsilon\Omega_L^2}{(\omega^2 - \Omega_L^2) + j\Gamma_L\omega}$$

where ω_D is the plasma frequency, γ_D the damping coefficient, Ω_L the oscillator strength, Γ_L spectral width of the Lorentz oscillator, and $\Delta\varepsilon$ is a weight factor.

This model implemented in an FDTD algorithm yields to accurate results in the range of wavelength from 500 to 1200 nm.[24]

Another problem arises when the FDTD method is used for the study of an anisotropic medium. It is well-known that the FDTD algorithm assumes that space is discretized so that each field quantity is available only at a unique location given by the Yee cell.

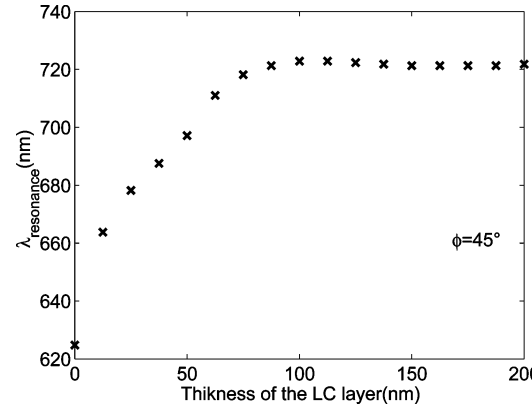

Figure 3. Effect of the thickness of LC layer on the LSPR.

For general anisotropic materials, the relation between $\vec{D}$ (electric flux) and $\vec{E}$ (electric field) is tensoriel and can be expressed as

$$\begin{bmatrix} D_x \\ D_y \\ D_z \end{bmatrix} = \varepsilon_0 \begin{bmatrix} \varepsilon_{xx} & \varepsilon_{xy} & \varepsilon_{xz} \\ \varepsilon_{yx} & \varepsilon_{yy} & \varepsilon_{yz} \\ \varepsilon_{zx} & \varepsilon_{zy} & \varepsilon_{zz} \end{bmatrix} \begin{bmatrix} E_x \\ E_y \\ E_z \end{bmatrix}$$

We notice that in order to compute for example D_x, we need to know the value of D_y and D_z at the same location as D_x. For this reason, we introduce a new set of approximations consisting on linar interpolation in order to deduce the value of D_y and D_z at the D_x location.[25] Analogue interpolations are made when computing D_y and D_z .

The structures of interest are periodic in the $x-y$ directions, and for this reason the computational volume is truncated with periodic boundary conditions. The normal-incidence periodic boundary conditions are easy to implement as the wavefront has no time delay, and the stability criteria is unchanged. In the z-direction, the computational volume is truncated with absorbing boundary conditions to simulate the extension of the lattice to infinity. This truncation is done by placing two UPML (uniaxial perfect matched layer) regions at top and bottom to absorb the waves. The UPML medium is adapted to the truncation of FDTD lattices, in wich the finite-difference equations can be used for the total computation domain by properly choosing the uniaxial parameters.[22]

All of our calculations are made with a spatial discretization $\Delta x = \Delta y = \Delta z = 3.125$ nm and a temporal discretization $\Delta t = 0.9\Delta x/((3)^{1/2}c)$ with c the velocity of light in vacuum.

Results and Discussions

Effect of the Thickness of the LC Layer on the LSPR Wavelengths. The LC which is the environment media of gold nanoparticles has an infinite dimension in x and y directions. In z-direction, this environment has a thickness d that can modify the plasmon resonance. For this reason we start by studying the effect of d on the plasmon resonance. Spectra are computed for normal incidence with a polarization along the x-axis (this will hold for all following calculations). The optical axis is in the $x-y$ plane with $\phi = 45°$. Results are presented in Figure 3. We observe an important red shift when we increase the thickness of the LC layer. The LSPR does not shift significantly when d exceeds 100 nm. This behavior was also observed in case of isotropic environment media, and the "saturation of the shift" is achieved when the distance between the top of the

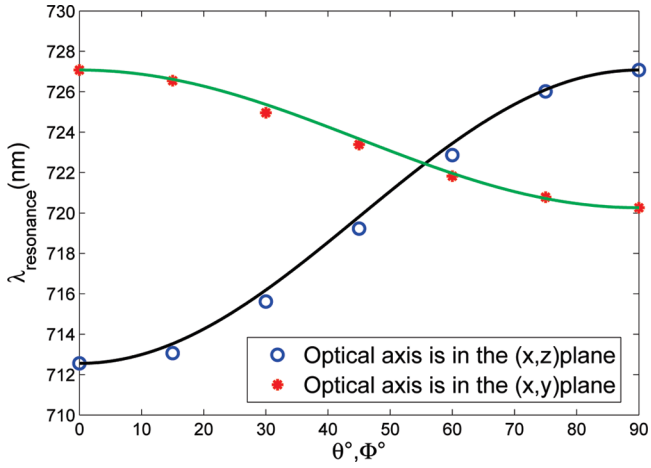

Figure 4. Effect of the orientation of the optical axis on the LSPR.

particle and the LC-air interface is almost equal to the decay length of the evanescent waves.[26]

Henceforth, the thickness d of LC layer will be maintained equal to 100 nm.

Effect of the Orientation of the Optical Axis on the LSPR Wavelength. The evolution of the position of the resonance as a function of the orientation of the director is presented in Figure 4.

As the angle θ (measured with respect to $\vec{z}$) is increased, we observe a red shift of the resonance. This is explained by the fact that the dipolar resonance condition along the long axis of the ellipsoid is modified. Indeed, in this case, the effective index for the extraordinary wave (polarized along the x-axis) is

$$n = \frac{n_o n_e}{\sqrt{n_e^2 \cos^2\theta + n_o^2 \sin^2\theta}} \tag{3}$$

meaning that when θ goes from 0° to $\theta = 90°$, the index varies from $n_o = 1.53$ to $n_e = 1.74$.

On the same figure, we also present results for the optical axis rotated in the $x-y$ plane. We observe a blue shift that is also simply explained by a modification of the dipolar resonance condition along the long axis of the ellipsoid, because in this case, the effective index for the extraordinary wave is

$$n = \frac{n_o n_e}{\sqrt{n_e^2 \sin^2\phi + n_o^2 \cos^2\phi}} \tag{4}$$

Thus this index varies from $n = n_e$ for $\phi = 0°$, to $n = n_o$ for $\phi = 90°$.

The fact that the blue shift is only half of the initial red-shift can be simply explained: in the initial state, there is no in-plane anisotropy, whereas when we rotate in the $x-y$ plane, the in-plane anisotropy is still the same. By rotating the optical axis in the $y-z$ plane, we would retrieve the initial state with a lowerig of the in-plane index hence a further blue shift of the resonance.

This two series of dots have a similar behavior and are fitted (continuous lines) with a function of the form[18]

$$\lambda_r = \lambda_0 + \Delta\lambda \sin^2\theta \tag{5}$$

with λ_0 the resonance wavelength obtained for $\theta = 0°$ (or $\phi = 0°$).

$\Delta\lambda_\theta = \lambda_{r,\theta=90°} - \lambda_{r,\theta=0°}$ (or $\Delta\lambda_\phi = \lambda_{r,\phi=90°} - \lambda_{r,\phi=0°}$) corresponds to the amplitude of the shift. The spectral sensitivity of the LSPR is the relative shift in resonance wavelength with respect to the refractive index change of surrounding materials,[5] and it is usually expressed as

$$S = \frac{d\lambda_r}{dn} \tag{6}$$

but in the case of LC surrounding media, n depends only on the orientation of the optical axis (θ or ϕ), so we will define S as $S_\theta = \partial\lambda_r/\partial\theta$ (or $S_\phi = \partial\lambda_r/\partial\phi$). Having in mind that λ_r is well described by equation eq 5, we deduce that

$$S_\theta = 2\Delta\lambda_\theta \sin\theta \cos\theta \tag{7}$$

Clearly we see that the sensitivity does not explicitly depend on the maximum wavelength itself ($\lambda_r|_\theta$) but on the difference $\Delta\lambda_\theta$ (or $\Delta\lambda_\phi$), defined as a spectral tunability. Note that increasing this spectral tunability means increasing sensitivity, which is required for example for biosensing applications. In fact, many theoretical and experimental studies currently focus on metal nanoparticles with different geometries to find the best nanoparticles configuration to enhance the sensitivity of the plasmon resonance response.[1,5,27−33] So, in the next section we will investigate the effect of geometrical parameters on the sensitivity of the plasmon response to a change of orientation of the director of the LC molecules surrounding the nanostructures.

Results presented here are in agreement with those obtained in our previous work,[18] where the nanostructures were gold cylinders with diameter $D = 100$ nm, $h = 50$ nm, and a periodicity $p_x = p_y = 200$ nm. However, we note that nanocylinders with elliptic basis are more sensitive to the orientation of the director as $\Delta\lambda_\theta$ is equal to +14.52 nm, while in the case of nanocylinders with circular basis $\Delta\lambda_\theta$ was equal to +11.5 nm. This difference is due to the "shape factor" as an elliptic shape exhibits more confinement of the electronic cloud leading to more sensitivity to the surrounding media,[1,4,5] despite a lowering of the volume[34] ($b = 50$ nm for ellipses, $b = 100$ nm for cylinders).

The same calculations were made for an incident polarization along the y-axis. In this case, very weak values of $\Delta\lambda_\theta$ or $\Delta\lambda_\phi$ were achieved (around 3 nm), meaning that the anisotropy between the x- and y-axis of the structure is still increased by using an anisotropic environment.

Improving Sensitivity

We will now focus on how we can increase the value of $\Delta\lambda_\theta$ ($= \lambda_{r,\theta=90°} - \lambda_{r,\theta=0°}$) to increase the sensitivity of the structure to the orientation of the director according to eq 7. From the previous section, we deduce that we cannot increase the spectral tunability $\Delta\lambda_\theta$ of our structure by increasing the z-dimension of the LC layer beyond 100 nm, as the LSPR position remains constant. But we can modify other geometrical parameters: the distance (edge to edge) between nonocylinders in the x-direction or y-direction, that will be noted respectively l_x and l_y, or the periodicity of the array in x-direction (respectively y-direction) noted p_x (respectively p_y).

We choose to start by checking the effect of modifying the major axis and the periodicity on the plasmon resonance wavelength. The polarization of the incident light is parallel to the x-axis and the optical axis is assumed to be parallel to the

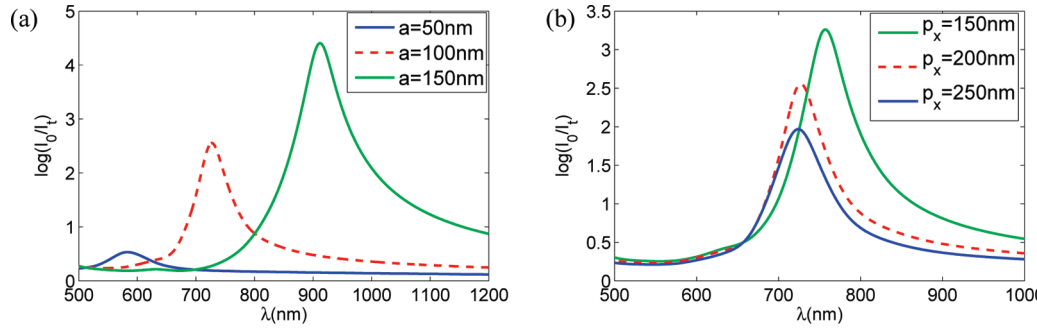

Figure 5. Shift of the LSPR induced by variation of geometrical parameters.

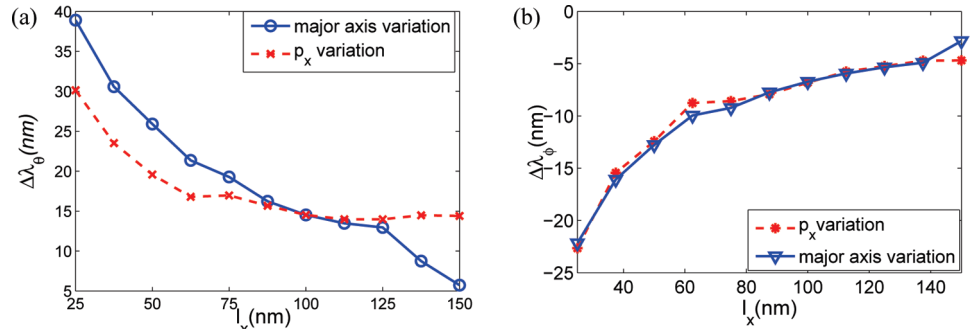

Figure 6. Effect of modifying geometrical parameters on spectral tunability.

x-axis ($\theta = 90°$ and $\phi = 0°$). Results are presented in Figure 5a,b. We observe an important red shift when we increase the major axis (leading to a decrease of l_x as p_x is constant), which is the well-known behavior for this kind of particles.[35] A similar but less pronounced behavior is observed when maintaing $a =$ 100 nm, $b = 50$ nm and decreasing the distance l_x by decreasing the periodicity p_x. This in turn confirms the fact that the shift observed in Figure 5a is mainly driven by the modification of the aspect ratio.

These results are similar to those obtained in the case of an isotropic surrounding material and one can be referred to many works that detail these shifts[3,4,36,37]

Figure 5 allows us to situate the plasmon resonance wavelength in the visible spectrum when modifying geometrical parameters, but our attention now will be reported on the sensitivity itself of the system to the orientation of the optical axis, quantified by the value of $\Delta\lambda_\theta$ or $\Delta\lambda_\phi$ (ie, S_θ and S_ϕ according to eq 7).

In a first step, to decrease l_x, we can simply decrease p_x (and maintain $p_y = 200$ nm, $a = 100$ nm, and $b = 50$ nm) to study the effect of coupling between nanoparticles on the sensitivity S_θ (see Figure 1b). Concretely, p_x will be varied from 125 to 250 nm, thus leading l_x to vary from 25 to 150 nm as $a = 100$ nm. Results are presented in Figure 6a with dashed lines. In this computation we assume that the optical axis is in the $x-z$ plane. We observe that $\Delta\lambda_\theta$ increases nonlinearly when l_x is decreased. This behavior is due to the increase of the "coupling" factor. When $l_x > 100$ nm, the sensitivity of the structures does not vary due to the disappearance of coupling between proximal nanoparticles.

In a second set of computation represented with a continuous line in Figure 6a, we decrease l_x by simply increasing the major axis a of the particle (and maintaining $p_x = p_y = 200$ nm and $b = 50$ nm), thus allowing us to examine the effect of the coupling between nonoparticle but also the volume effect due to the modification of the major axis. We observe that $\Delta\lambda$ also increases when l_x is decreased, and its value is more important due to the cumulating of volume factor and coupling factor. The best spectral tunability observed is 40 nm, which is three times higher than the value achieved with initial parameters. Note that the variation of the major axis is from 50 to 175 nm, leading l_x to vary also from 25 to 150 nm.

Similar behaviors are observed when focusing on $\Delta\lambda_\phi$ (i.e., spectral tunability resulting by rotating the director in the $x-y$ plane) and results are presented in Figure 6b. We observe that when the optical axis is in the $x-y$ plane, decreasing l_x leads also to a no linear increasing of the sensitivity to the orientation of the LC director. The spectral tunability reaches in this case -23 nm, so this configuration is less sensitive than the previous one, which could be expected from our first calculations depicted in Figure 4.

We can thus conclude that coupling factor and volume factor contribute to enhance the sensitivity of the LSPR to the orientation of the LC molecules, and the distance l_x between proximal nanoparticle in the coupling direction (in this case x-direction) allows us to modulate this sensitivity.

Validity of Our Approach

In our simulations, we neglect interface effects called the anchoring phenomenon, which is the tendency of a liquid crystal to orient in a particular direction when it is in contact with confining surfaces (metal). It seems that the influence of this phenomena would be mainly a broadening of the plasmon resonance, as pointed out by Kossyrev et al.[12]

On the contrary to experimental results achieved by increasing the external electric field from zero up to a threshold value for which all LC molecules are aligned along the field,[10,12−15] we assume that the electric field is always present with a strength sufficient to align all molecules and that its direction may be freely changed.

From this last assumption, a lowering of $\Delta\lambda$ (spectral tunability) should also be expected. Nevertheless, we believe that the main features that we have observed (λ_r as a function of the orientation of optical axis and $\Delta\lambda$ as a function of different geometrical parameters) would be preserved.

Conclusion

FDTD simulations of plasmon resonance of gold nanoparticles embedded in a nematic liquid crystal layer were performed. It was shown that these structures act as active plasmonic devices, as we are able to control and tune the plasmon resonance by simply rotating the optical axis. This spectral tunability can be increased by modifying geometrical parameters. We have shown that for light polarized parallel to the major axis of the elliptic basis the absolute value of the plasmon resonance sensitivity increases nonlinearly when the distance between gold nanoparticles is decreased.

The most suitable configuration is when we rotate the director in the $x-z$ plane and decrease the distance between particles in x direction by increasing the major axis. The spectral tunability reaches 40 nm in this case. Thus, we suggest that this configuration is well adapted for sensing applications.

Acknowledgment. The authors acknowledge financial support by the ANR project NP/CL. M.D. acknowledges the Regional Council of Champagne-Ardenne for financial support.

References and Notes

(1) Maier, S. A. *Plasmonics Fundamentals and Applications*; Springer: New York, 2007.
(2) *Surface Plasmon Nanophotonics*; Brongersma, M. L., Kik, P. G., Eds.; Springer: New York, 2007.
(3) Grimault, A. S.; Vial, A.; Lamy de la Chapelle, M. *Appl. Phys. B* **2006**, *84*, 111–115.
(4) Jain, P. K.; Lee, K. S.; El-Sayed, I. H.; A. El-Sayed, M. *J. Phys. Chem. B* **2006**, *110*, 7238–7248.
(5) Lee, K. S.; El-Sayed, M. A. *J. Phys Chem. B* **2006**, *110*, 19220–19225.
(6) Ibn El Ahrach, H.; Bachelot, R.; Vial, A.; Lerondel, G.; Plain, J.; Royer, P.; Soppera, O. *Phys. Rev. Lett.* **2007**, *98*, 107402.
(7) Abdulhalim, I. *J. Opt. A: Pure Appl. Opt.* **2009**, *11*, 015002.
(8) Li, Y.; Sun, J.; Wang, L.; Zhan, P.; Cao, Z.; Wang, Z. *Appl. Phys. A* **2008**, *92*, 291–294.
(9) Ojima, M.; Numata, N.; Ogawa, Y.; Murata, K.; Kubo, H.; Fujii, A.; Ozaki, M. *Appl. Phys. Express* **2009**, *2*, 086001.
(10) Hsu, L. H.; Lo, K. Y.; Huang, S. A.; Huang, C. Y.; Yang, C. S. *Appl. Phys. Lett.* **2008**, *92*, 181112.
(11) Park, S. Y.; Stroud, D. *Condens. Mater.* **2005**, *1*, 217401.
(12) Kossyrev, P. A.; Yin, A.; Cloutier, S. G.; Cardimona, D. A. *Nano Lett.* **2005**, *5*, 1978–1981.
(13) Evans, P.; Wurtz, G. A.; Hendren, W. R.; atkinson, R.; Dickson, W.; Zayats, A. V.; Pollard, R. J. *Appl. Phys. Lett.* **2007**, *91*, 043101.
(14) Chu, K. C.; Chao, C. Y.; Chen, Y. F.; Wu, Y. C.; Chen, C. C. *Appl. Phys. Lett.* **2006**, *89*, 103107.
(15) Zheng, Y. B.; Hsiao, V. K. S.; Huang, T. J. *Proc. - IEEE Micro Electro Mech. Syst.* **2008**, *978*, 705–708.
(16) Hsiao, V.; Zheng, Y.; Juluri, B.; Huang, T. *Adv. Mater.* **2008**, *20*, 3528–3532.
(17) Dickson, W.; Wurtz, G. A.; Evans, P. R.; Pollard, R. J.; Zayats, A. V. *Nano Lett.* **2008**, *8*, 281–286.
(18) Dridi, M.; Vial, A. *Opt. Lett.* **2009**, *34*, 2652–2654.
(19) Oswald, P.; Pieranski, P. *Nematic and Cholesteric Liquid Crystals*; Taylor and Francis Group: London, 2005.
(20) Born, M.; Wolf, E. *Principle of Optics*, 6th ed.; Pergamon Press: Oxford, 1980.
(21) Yee, K. *IEEE Trans. Antenn. Propag.* **1966**, *14*, 302–307.
(22) Taflove, A.; Hagness, S. C. *Computational Electrodynamics: The Finite-Difference Time Domain Method*, 2nd ed.; Artech House: Boston, 2000.
(23) Kunz, K. S.; Luebbers, R. J. *The Finite-Difference Time-Domain Method for Electromagnetics*; CRC Press: New York, 1993.
(24) Vial, A.; Grimault, A. S.; Macias, D.; Barchiesi, D.; Lamy de la Chapelle, M. *Phys. Rev. B* **2005**, *71*, 085416.
(25) Dou, L.; Sebak, A. R. *Microwave Opt. Technol. Lett.* **2006**, *48*, 2083–2090.
(26) Grimault, A. S.; Vial, A.; Grand, J.; Lamy de la Chapelle, M. *J. Microscopy* **2008**, *229*, 428–432.
(27) Haes, A. J.; Duyne, R. P. V. *J. Am. Chem. Soc.* **2002**, *124*, 10596–10604.
(28) McFarland, A. D.; Duyne, R. P. V. *Nano Lett.* **2003**, *3*, 1057–1062.
(29) Ribon, J. C.; Haes, A. J.; McFarland, A. D.; Yonzon, C. R.; Duyne, R. P. V. *J. Phys. Chem. B* **2003**, *107*, 1772–1780.
(30) Raschke, G.; Brogl, S.; Susha, A. S.; Rogach, A. L.; Klar, T. A.; Feldmann, J. *Nano Lett.* **2004**, *4*, 1853–1857.
(31) Zhao, L.; Kelly, K. L.; Schatz, G. C. *J. Phys Chem. B* **2003**, *107*, 7343–7350.
(32) Tam, F.; Moran, C.; Halas, N. *J. Phys. Chem. B* **2004**, *108*, 17290–17294.
(33) Link, S.; Wang, Z. L.; El-Sayed, M. A. *J. Phys. Chem. B* **1999**, *103*, 3529–3533.
(34) Grand, J.; Adam, P.-M.; Grimault, A.-S.; Vial, A.; Lamy de la Chapelle, M.; Bijeon, J.-L.; Kostcheev, S.; Royer, P. *Plasmonics* **2006**, *1*, 135–140.
(35) Kelly, K.; Coronado, E.; Zhao, L. L.; Schatz, G. C. *J. Phys. Chem. B* **2003**, *107*, 668–677.
(36) Zhang, Z. Y.; Zhao, Y. P. *J. Appl. Phys.* **2007**, *102*, 113308.
(37) Rechberger, W.; Hohenau, A.; Leitner, A.; Krenn, J. R.; Lamprecht, B.; Aussenegg, F. R. *Opt. Commun.* **2003**, *220*, 137–141.

JP910950M